A Delayed Detached Eddy Simulation Model for the Simulation of Complex Turbulent Flow

L. J. Zhai[1], H. X. Chen[1†] and Z. Ma[2]

[1] Shanghai Key Laboratory of Mechanics in Energy Engineering, Shanghai Institute of Applied Mathematics and Mechanics, School of Mechanics and Engineering Science, Shanghai University, Shanghai, Shanghai 200072, China
[2] Chinese Ship Scientific Research Center, Shanghai, Shanghai 200011, China

†*Corresponding Author Email: chenhx@shu.edu.cn*

ABSTRACT

A new turbulent model based on Delayed Detached Eddy Simulation (DDES) with non-linear eddy viscosity model (NLEVM) was developed to predict the complex turbulent flow. The numerical simulation of the triangular cylinder and the centrifugal pump was carried out to investigate the ability and applicability of the DDES model based on NLEVM (DDES_NL). Compared to the turbulent model based on the eddy viscosity model, the computational results of the triangular cylinder showed the advantage of the non-linear eddy viscosity modification in the DDES_NL model which can improve the accuracy of the prediction in the flow phenomenon with a relatively simple turbulence structure. Regrettably, some small-scale turbulent structures among those still cannot be captured accurately. The numerical simulation of the centrifugal pump predicted by the DDES_NL model shows more abundant flow structures and gets close to the realistic statistical characteristics. It also proves the good applicability of the DDES_NL model in complex flow. This study aims to contribute to the growing area of turbulence modeling by exploring it.

NOMENCLATURE

K	turbulent kinetic energy	DDES	Delayed Detached Eddy Simulation
P	static pressure	NLEVM	Non-Linear Eddy Viscosity Model
P_k	turbulent kinetic energy production	DDES_NL	DDES model based on NLEVM
ε	turbulent dissipation rate	RANS	Reynolds-averaged Navier-Stokes
μ, μ_t	laminar and eddy viscosities	LES	Large Eddy Simulation
v, v_t	laminar and eddy kinematic viscosities	DNS	Direct Numerical Simulation
ρ	density	DES	Detached Eddy Simulation
$\bar{u}$	mean velocity	MSD	Modelled Stress Depletion
$\bar{p}$	mean pressure	SST	Shear-Stress Transport (model)
δ_{ij}	unit vector	URANS	Unsteady RANS
P	static pressure		

1. INTRODUCTION

With the fast development of computational fluid dynamics (CFD), numerical simulation methods have been emerging as a wide range of research turbulent flows. At present, the popular numerical simulation methods are Reynolds-averaged Navier-Stokes (RANS) simulations based on the assumption of linear vortex viscosity coefficients, as a result they significantly reduce the time for turbulence calculations (Ma *et al.* 2009). The eddy viscosity model has performed well in applications. However, it is less valid for flows with high mean shear rates or huge separations. The model also has the problem of not capturing the scale effects of transient flows due to the inherent damping of unsteady motion (Tucker 2011a; Zhang *et al.* 2010; Zhu *et al.* 2014).

Large eddy simulations (LES) can be solved for a range of turbulence scales, and subgrid-scale eddy models can capture unsteady flow characteristics more accurately (Zhang *et al*. 2015; Tucker 2011b). An accuracy LES should solve all turbulence scales in the flow, including the majority of turbulent kinetic energy and Reynolds shear stress in the Local area (Vengadesan and Nithiarasu 2007). In LES simulations, the scales in the turbulence spectra that are approximately proportional to the wall separation are very tiny in the wall boundary layer and hence demand an overly high resolution, almost as high as direct numerical simulation (DNS). Thus, it is not viable to simulate high Reynolds number flows with LES in industry applications.

The RANS/LES hybrid methods have attracted a great deal of interest since their inception, and many investigators have produced a wide variety of hybrid methods (Froehlich and Terzi 2008; Zhang *et al*. 2022). The most widely used of these is the detached eddy simulation (DES) model. Spalart *et al*. (1997) proposed the SA-DES model in 1997, which regressed to the RANS model in the near-wall area and showed the features of the LES solution in the far-wall area. Subsequently, Strelets (2001) adopted a similar idea to build the SST-DES model which was based on the SST two-sided equation model presented by Menter. The DES model has shown great suitability for separate flows, but it also has some deficiencies (Spalart 2009). A typical issue is Modelled Stress Depletion (MSD), which is primarily caused by inappropriate mesh densification in the boundary layer. As a result of improper mesh desensitization in the boundary layer (mostly in the flow direction and span direction), the RANS/LES interface moves to the wall and the RANS modeled area decreases. Nevertheless, the mesh resolutions do not support an exact resolution of the LES model at this point. If the calculated stresses are so small, the MSD issue arises. The MSD issue can lead to a reduction in calculated wall friction. In severe cases early separation or non-physical separation can occur. To resolve this problem, Menter and Kuntz (2003) presented a way to reduce the overdependence on the mesh density by introducing a delay function F_{sst}. Menter's delay function is based on a two-squared SST model. Though it can model the actual flow field more accurately than the original DES model; it is not universal, for this reason, Spalart *et al*. (2006) constructed a generally applicable delay function that was first adopted to the original DES RANS/LES conversion function. These improvements effectively delayed the conversion from RANS to LES and resolved the separation problem due to the mesh in the original DES (Chauvet *et al*. 2007; Fu *et al*. 2007; Trapier *et al*. 2008). The Delayed Separation Eddy Simulation (DDES) model covered the boundary layer in RANS mode and the lightly separated boundary layer, thereby avoiding the high cost of solving wall turbulence.

Many scholars have used DDES to conduct numerical simulation studies. Liu *et al*. (2017) used DDES to study the non-constant flow characteristics of the leaf-grid separation vortex and found that the change of leaf-grid geometric parameters and angle of attack had a significant effect on the vortex motion of the flow field. The basic flow phenomena of the transonic high-pressure turbine guide vane LS89 were researched separately by Lin *et al*. (2016) with the help of the DDES method, which demonstrated that the DDES method has strong discriminative power and computational reliability for the non-constant structure. Yin *et al*. (2015) proposed the implementation of a dynamic procedure to locally compute the value of the model constant C_{DES}, as used in the eddy simulation branch of Delayed Detached Eddy Simulation. Liu and Tong (2015) used the delayed separation vortex simulation method to study the aerodynamic noise characteristics of cavities and cavities with hatches and showed that DDES has strong accuracy for the simulation of aerodynamic noise problems. Hu *et al*. (2017) simulated the large-angle 6:1 ellipsoidal winding flow and low-speed large-angle delta wing winding flow using the DDES-SST method, and observed vortex characteristics that matched the actual phenomenon, while the calculated results were consistent with the experimental data. Du *et al*. (2017) studied the performance characteristics of the DDES delay function, and the results showed that there are significant differences in the solving ability and action range of different delay functions, and DDES-F_1 mainly plays a protective role, and the numerical prediction is similar to the experimental data. Zhang *et al*. (2016) used the DDES-SA turbulence model, mainly to verify its accuracy, to numerically simulate the flow field of delta wing winding, and found that the numerical prediction results were matching with the experimental data. Hu *et al*. (2021) adopted detached-eddy simulations with the shear stress transfer k-ω turbulence model, the Ffowcs Williams–Hawking's acoustics model, and the Schnerr–Sauer cavitation model predicted the contra-rotating propellers noise radiation. Li *et al*. (2021) adopted dynamic delayed detached-eddy simulations of the turbulent wall heat transfer behind a wall-proximity square rib, purposing to clarify unsteady flow behaviors and their influence on wall heat transfer. Shi and Kollmann (2021) investigated a novel trailing-edge treatment to minimize trailing-edge noise. Improved delayed detached eddy simulations are performed to contrast the aeroacoustic performance of a porous wavy trailing edge to those of clean airfoil, porous trailing edge, and wavy trailing edge. From the literature review, much of the research up to now has been using the DDES model to simulate the model numerically. Since the DDES model is based on the linear vortex viscosity model, however, it has low prediction accuracy for flow problems with large pressure gradients, so in this paper, a new turbulent model based on Delayed Detached Eddy Simulation (DDES) with non-linear eddy viscosity model (NLEVM) was developed.

In this study, a DDES model based on NLEVM was introduced. To verify the ability and

applicability of the DDES_NL model, numerical simulations were performed around a simple geometry triangular cylinder flow and found that in better agreement with the experimental results. Then numerical simulations were performed in a rotating simple geometry channel flow and were found to be closer to the DNS results. Finally, simulations were performed in a centrifugal pump with a complicated rotating structure and found to be able to capture more abundant flow structures. In summary, these results show the usefulness of turbulence models.

2. THE DDES MODEL BASED ON NLEVM (DDES_NL)

2.1 Non-linear eddy viscosity model (NLEVM)

The Navier–Stokes (NS) equations are employed to describe the incompressible turbulent flow, where the continuity and momentum equations are expressed as follows:

$$\frac{\partial \overline{u_i}}{\partial x_i} = 0 \tag{1}$$

$$\frac{\partial \left(\rho \overline{u_i} \right)}{\partial t} + \frac{\partial \left(\rho \overline{u_i u_j} \right)}{\partial x_j} = $$
$$-\frac{\partial \overline{p}}{\partial x_i} + \frac{\partial}{\partial x_i} \left(\mu \frac{\partial \overline{u_i}}{\partial x_i} - \rho \overline{u_i' u_j'} \right) \tag{2}$$

In these equations, $\overline{u}$ denotes the mean velocity, $\overline{p}$ denotes the mean pressure, ρ is the density, and μ is the dynamic viscosity. The subscripts (i, j, k) denote the directions of the Cartesian coordinates, and $-\overline{u_i' u_j'}$ are the Reynolds stresses. According to the Boussinesq assumption, the Reynolds stress tensor is given by

$$-\rho \overline{u_i' u_j'} = -\mu_t \left(\frac{\partial \overline{u_i}}{\partial x_j} + \frac{\partial \overline{u_j}}{\partial x_i} \right) + \frac{2}{3} \delta_{ij} k \tag{3}$$

Where δ_{ij} denotes the Kronecker delta, k denotes the turbulent kinetic energy. Where μ_t denotes the eddy viscosity, as follows:

$$\mu_t = C_\mu \frac{\rho k^2}{\varepsilon} \tag{4}$$

Where ε is the turbulent dissipation rate, C_μ denotes the eddy viscosity coefficient. According to the results of experiments (Champagne *et al.* 1970; Tavoularis and Corrsin 1981) and the DNS (Lee *et al.* 1990; Rogers and Moin 1987), the non-linear eddy viscosity model had been proposed by Wei *et al.* (2016) and was applied first to investigate the pressure fluctuation characteristics of the centrifugal pump.

The expression of the eddy viscosity coefficient C_μ which is a piecewise function read is evaluated as:

$$C_\mu = 0.00099 + \begin{cases} A \\ B \end{cases}$$

$$A = \frac{0.09401}{\left(1 + \left(\frac{\eta}{5.2} \right)^{6.1} \right)}, \eta \le 4.4$$

$$B = 0.2 \times \exp(-\frac{\eta}{3.05}) + 0.03 \times \exp(-\frac{\eta}{15.5}), \eta \ge 4.4$$

$$\tag{5}$$

$$\eta = \sqrt{\frac{1}{2}(\tilde{S}^2 + \tilde{\Omega}^2)} \tag{6}$$

$$\tilde{S} = \sqrt{2\tilde{S}_{ij}\tilde{S}_{ij}} \ , \ \ \tilde{S}_{ij} = \frac{k}{\varepsilon} S_{ij} \tag{7}$$

$$\tilde{\Omega} = \sqrt{2\tilde{\Omega}_{ij}\tilde{\Omega}_{ij}} \ , \ \ \tilde{\Omega}_{ij} = \frac{k}{\varepsilon} \Omega_{ij} \tag{8}$$

Nonlinear eddy viscosity models can capture unsteady turbulent structures with excellent prediction precision, which has been demonstrated for unsteady flows around triangular cylinders, wind turbine wings, and 2D and 3D centrifugal pumps (Wei *et al.* 2015; Wei *et al.* 2017; Zhang *et al.* 2019a,b).

2.2 DDES type model based on SST k-ω model

Although the DES model was applied first to the S-A one-equation RANS model by Spalart (2009), Travin *et al.* (2000) summarized a general construction model for the DES approach: a DES model based on any RANS model can be obtained by simply making appropriate modifications to the turbulence length scale of that model, and either implicitly or explicitly included in any RANS model. First proposed by Strelets (2001) in 2001, also obtained by this model, the model construction model is as follows:

For the SST k-ω model, the turbulence length scale l_{SST} is given by:

$$l_{SST} = \frac{\sqrt{k}}{\beta^* \omega} \tag{9}$$

The turbulence length scale of the DES model is given by:

$$l_{DES} = \min \left(l_{SST}, C_{DES} \Delta \right) \tag{10}$$

Among them, the model constant is calibrated $C_{DES} = 0.61$. Considering that the equation should be as concise as simple and that the role of the sub-grid-scale eddies modeled is not crucial in the overall flow field simulation, the DES model only modifies the turbulence scale in the dissipation term D_k of the k-equation of the SST k-ω model. Combining formula (9) and denote D_k, it is transformed into the following equation:

$$D_k = \frac{\rho k^{\frac{3}{2}}}{l_{SST}} \qquad (11)$$

Add function F_{DES} (hereinafter the coefficient is termed the model switching function):

$$\frac{\rho k^{\frac{3}{2}}}{l_{SST}} \rightarrow \frac{\rho k^{\frac{3}{2}}}{l_{SST}} \cdot F_{DES} \qquad (12)$$

For any two-equation RANS model, the general form of F_{DES} is given by:

$$F_{DES} = \max\left(\frac{l_{RANS}}{l_{LES}}, 1 \right) \qquad (13)$$

Here is the Reynolds time-average scale $l_{RANS} = l_{SST}$, therefore the control equation of the SST k-ω model is transformed into the following equation:

$$\frac{\partial(\rho k)}{\partial t} + \frac{\partial(\rho u_j k)}{\partial x_j} = \tilde{P}_k - \beta^* \rho k \omega F_{DES}$$
$$+ \frac{\partial}{\partial x_j}[(\mu + \sigma_k \mu_t) \frac{\partial k}{\partial x_j}] \qquad (14)$$

$$\frac{\partial(\rho \omega)}{\partial t} + \frac{\partial(\rho u_j \omega)}{\partial x_j} = \alpha \rho S^2 - \beta \rho \omega^2 +$$
$$\frac{\partial}{\partial x_j}[(\mu + \sigma_\omega \mu_t) \frac{\partial \omega}{\partial x_j}] + 2(1-F_1)\rho \sigma_{\omega 2} \frac{1}{\omega} \frac{\partial k}{\partial x_j} \frac{\partial \omega}{\partial x_j} \qquad (15)$$

The formula is the DES model control equation based on SST k-ω. From equation (15), we can see that F_{DES} is related to l_{RANS} and l_{SST},

$$l_{RANS} = \sqrt{k} / \beta^* \omega, l_{LES} = C_{DES}\Delta.$$

(1) When $l_{RANS} < l_{LES}$, $F_{DES} = 1$, the control equation (13) is restored to the formula SST k-ω model;

(2) When $l_{RANS} > l_{LES}$, $F_{DES} = \sqrt{k} / \beta^* \omega / C_{DES}\Delta$, the k equation of the DES model is transformed into the following equation:

$$\frac{\partial(\rho k)}{\partial t} + \frac{\partial(\rho u_j k)}{\partial x_j} = \tilde{P}_k - \frac{\rho k^{\frac{3}{2}}}{C_{DES}\Delta}$$
$$+ \frac{\partial}{\partial x_j}[(\mu + \sigma_k \mu_t) \frac{\partial k}{\partial x_j}] \qquad (16)$$

Equation (16) is expressed in the form of sub-grid-scale eddies modeled. Since most of the region within the boundary layer is a flow with a low degree of turbulence, $\sqrt{k} / \beta^* \omega < C_{DES}\Delta$. Therefore the DES model based on the SST k-ω model is mainly in SST k-ω mode within the boundary layer,

and other regions are reflected in LES mode. The switch function setting mainly affects the switch position of the RANS model and LES model. If the setting is improper, the DES model will not work according to the set partition mode or cause problems such as grid-induced separation, affecting calculation accuracy. The function of the delay function is to delay the switch from the RANS model to the LES model in the boundary layer so that the entire boundary layer is simulated by the RANS model, to solve the problem of grid-induced separation. Aiming at the DES model based on SST k-ω, Du *et al.* (2017) compared the performance of three delay functions F_1 (first-order blending factor), F_2 (Second-order blending factor) and f_d (The empiric blending factor), and found that F_1 is a better balance between the solution accuracy and the role of the delayed RANS in the boundary layer, so in current work, the delay function is chosen as, which obtained by the following equation:

$$F_{DES} \rightarrow F_{(Delayed)DES} \qquad (17)$$

$$F_{(Delayed)DES} = \max\left(\frac{l_{RANS}}{l_{LES}} \cdot (1-F_1), 1 \right) \qquad (18)$$

From the function of the delay function, its main scope of action is in the boundary layer, so it should have a calibrated boundary, the function of the layer. The first-order blending factor F_1 of the SST k-ω model has the following equation:

$$F_1 \in (0,1) \qquad (19)$$

$$\begin{cases} F_1 \rightarrow 1 & (\text{Near-wall boundary area}) \\ F_1 \rightarrow 0 & (\text{Away from the mainstream area}) \end{cases} \qquad (20)$$

The values of these two functions are between 0 and 1, it was close to 1 in the near-wall area, it was away from the mainstream area of the wall close to 0. Therefore, F_1 is close to 1 in the boundary layer and close to 0 in other regions. Analytical formula (18), the introduction of ($1 - F_1$) makes the most area of the boundary layer close to the wall, at this time $l_{RANS} \div l_{LES} \cdot (1-F_1) < 1$, when $F_{(Delayed)DES} = 1$, the vast majority of the region in the boundary layer is the RANS control region.

3. NUMERICAL CALCULATION MODEL VALIDATION

3.1 Triangular cylinder

The flow around a triangular cylinder is a typical example of unsteady flows. The size of the computational domain is $20a \times 6a \times 6a$ in the streamwise (x), wall-normal (y), and spanwise (z) directions, respectively, shown in Fig. 1, where the distance from the inlet to the triangle is $4a$ and the distance from the outlet to the triangle is $15a$. With $188 \times 80 \times 80$ cells in respective directions, where
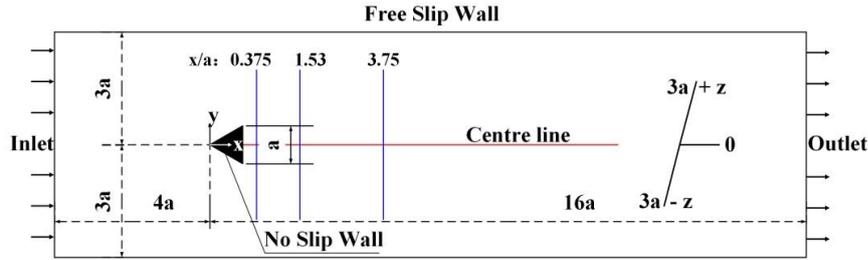
Fig. 1. Computational domain in the present study.

Table 1. Boundary conditions for the computational domain.

Boundary	Type	Velocity components	Pressure
Inlet	Inflow	$u_x = U, u_y = u_z = 0$	$\partial p / \partial n = 0$
Outlet	Outflow	$\partial u_i / \partial n = 0$	$p = 0$
Top and bottom	Free-slip	$\partial u_i / \partial n = 0$	$\partial p / \partial n = 0$
Front and back	Periodic	$u_i(x, y, z = 0, t) = u_i(x, y, z = L_z, t),$ $\partial u_i / \partial z(x, y, z = 0, t) = \partial u_i / \partial z(x, y, z = L_z, t)$	$p(x, y, z = 0, t) = p(x, y, z = L_z, t),$ $\partial p / \partial z(x, y, z = 0, t) = \partial p / \partial z(x, y, z = L_z, t)$
Cylinder	No-slip	$u_i = 0$	$\partial p / \partial n = 0$

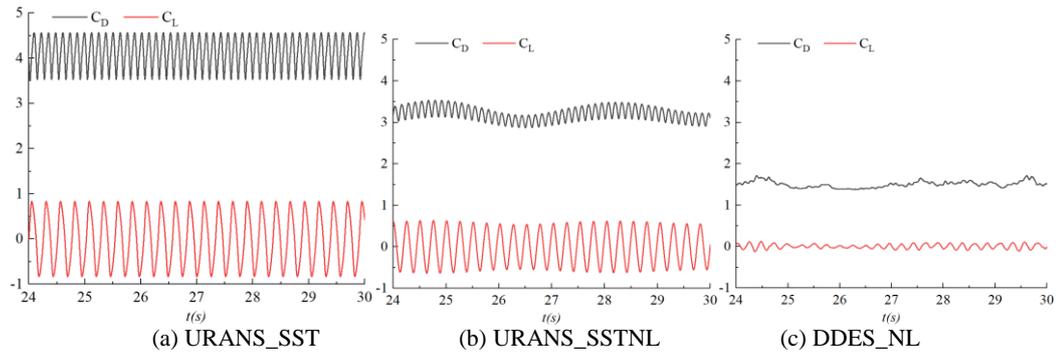| (a) URANS_SST | (b) URANS_SSTNL | (c) DDES_NL |

Fig. 2. Time history of the drag and lift coefficients.

the edge length(a) of the triangle is 1m (Wei *et al.* 2016). There are 1.47×10^6 hexahedral cells in the overall grids. The Reynolds number based on freestream velocity and edge length is 45500 and the inlet velocity is 17.3 m/s. The boundary conditions are listed in Table 1, which $\partial / \partial n = 0$ denotes zero normal gradient conditions. The time step size is set to 10^{-3} and the total time is set to 30s, with the initial values of corresponding steady simulation results. The numerical simulation is conducted based on the commercial software ANSYS CFX. The codes of the unsteady RANS models based on the NLEVM (URANS_SSTNL) model and DDES_NL model are embedded in ANSYS CFX by CFX Expression Language (CEL).

The unsteady RANS model (URANS_SST), URANS_SSTNL, and DDES_NL methods are used to simulate the triangular cylinder flow. The Strouhal number can be obtained by performing a fast Fourier transform on the time series of the lift coefficients. The drag and lift coefficients are expressed is given by

$$C_D = \frac{2 f_D}{\rho \times U_{in}^2 \times a \times Span} \quad (21)$$

$$C_L = \frac{2 f_L}{\rho \times U_{in}^2 \times a \times Span} \quad (22)$$

Where f_D and f_L are the drag and lift forces exerted on the triangular cylinder surface by the ambient fluid, moreover they can be obtained by integrating the pressure and shear stresses along with the streamwise and transverse directions, respectively. The time history of the drag and lift coefficient is presented in Fig. 2. The drag coefficient fluctuates by cause of the vortex shedding in the shear layer. it is evident that both the drag and lift coefficients oscillate periodically, the C_L has fluctuated around 0, nevertheless, the C_D has fluctuated around 4.114 by the URANS_SST model, the C_D has fluctuated around 3.206 by the URANS_SSTNL model, the C_D has fluctuated around 1.621 by the DDES_NL model. The experimental drag coefficient and Strouhal number are not available, but those of the same order of

Table 2. Drag coefficients and Strouhal number.

Data Sources	Re	C_D	St	Data type
Htun. (2004)	3×10^4	1.36	0.230	Exp
Zhu .(2014)	4.55×10^4	1.73	0.238	LES_WALL
In this paper	4.55×10^4	4.114	0.208	URANS_SST
		3.206	0.231	URANS_SSTNL
		1.621	0.239	DDES_NL

(a) URANS_SST

(b) URANS_SSTNL

(c) DDES_NL

(d) Exp (Htun M M. 2004;Wei *et al.* 2016)
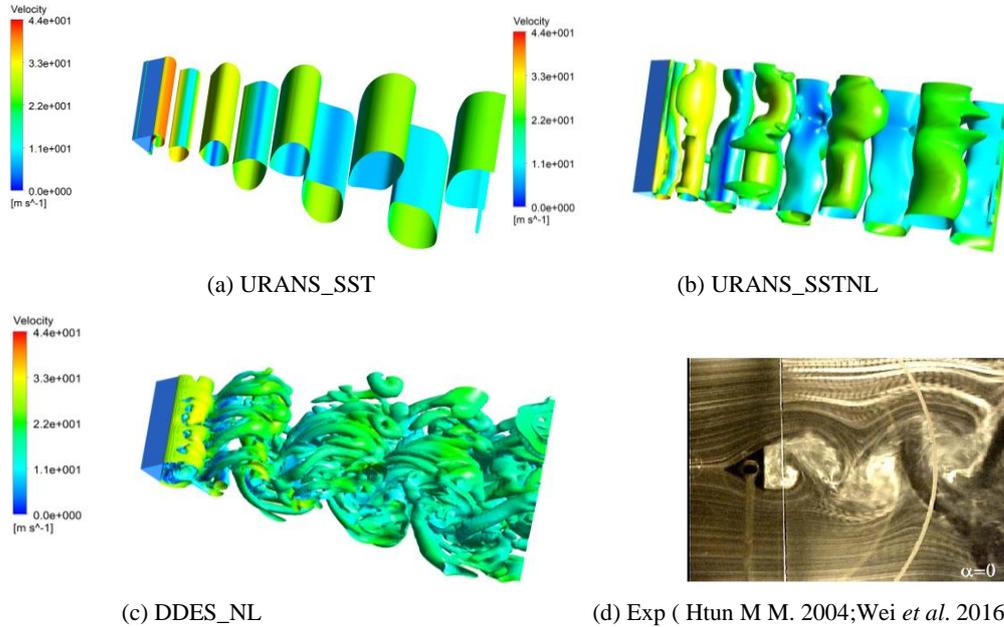
**Fig. 3. (Color online) Flow structures for flow around a triangular cylinder.**

magnitude ($Re = 3.00\times10^4$) (Htun 2004) are very close, which can be used for reference. The results listed in Table 2 show that the calculated drag coefficients are commonly larger than the experimental values, with the discrepancy of the URANS_SST model the largest, over three times the experimental value. The URANS_SSTNL model diminishes deviation, but the DDES_NL model offers the smallest discrepancy. Figure 3 shows the comparison of the calculated turbulent structures and the experimental (Htun 2004; Wei *et al.* 2016) (The second invariant of velocity gradient tensor is used to describe (Q-criterion($Q = S^2 - \Omega^2$, S being the strain rate and Ω the vorticity))), Htun M studied the influence of the size and direction of the top angle and the angle of attack on the structure of the flow through the triangular cylinder in a wind tunnel and conducted an experimental study; colored according to the velocity), it is apparent that all models can capture the periodic vortex shedding, the conventional URANS method only obtains the vortex structure of a single mode, while the DDES_NL method exhibits the ability to automatically detect the separation zone and switch to the LES mode for solving in the separation zone, thus capturing a richer large-scale turbulence structure.

Figure 4 shows the time-averaged axial velocity along the centreline behind the cylinder in comparison with the experimental data (Sjunnesson *et al.* 1992; Menter and Egorov 2010). The study by Sjunnesson was motivated by the application to flame holders. The Validation Rig is built in modules in order to simplify any modification of configuration or alteration of the optical access. In order to obtain a uniform flow upstream of the flame holder, some honeycombs and a Mach plate were placed in the upstream flow. The DDES_NL model results were in good agreement with the experimental results. The same is true for the comparison of the velocity profiles at
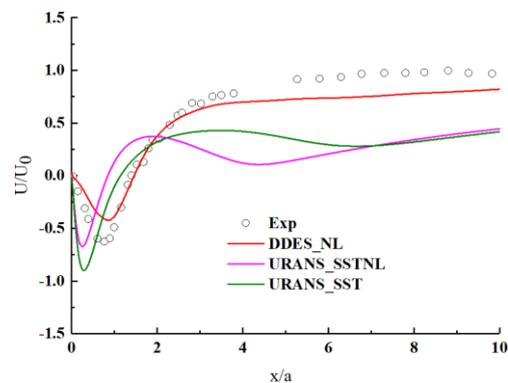
Fig. 4. Mean axial flow velocity along the centreline behind the triangular cylinder.

(a) x/a=0.375

(b) x/a=1.53

(c) x/a=3.75
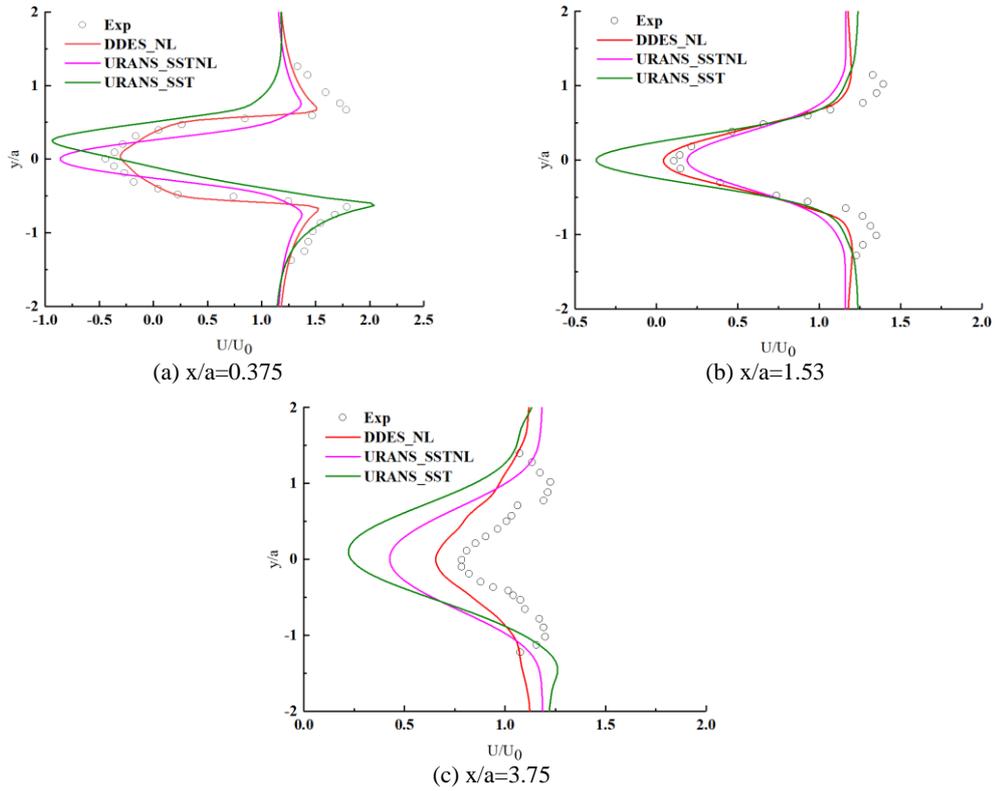
Fig. 5. Velocity profiles for three different stations downstream of the triangular cylinder.

(a) x/a=0.375
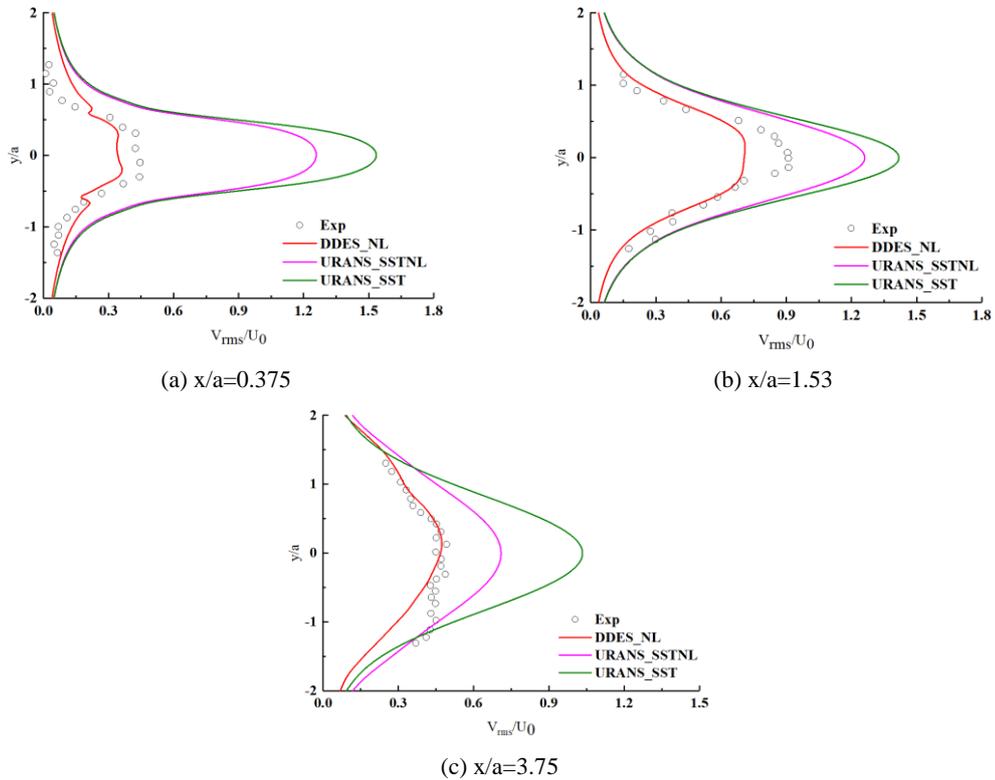
(b) x/a=1.53

(c) x/a=3.75

Fig. 6. Turbulence velocity profiles for three different stations downstream of the triangular cylinder.

three different stations (x/a = 0.375, x/a = 1.530, x/a = 3.750) shown in Fig. 5 and Fig. 6. It is concluded that the results of the DDES_NL model match well with the experimental values, both the URANS_SST model and the URANS_SSTNL model fail to simulate the flow behind the cylinder correctly.

Figure 7 displays the contours of the eddy viscosity and the turbulence kinetic energy on the central plane. The images show that the DDES_NL model predicts the lowest vortex viscosity and turbulent kinetic energy in the rear region of the triangular cylinder, followed by the URANS_SSTNL model and finally the URANS_SST model. The analysis suggests that the URANS_SST model vortex viscosity is larger and thus decays quickly at small scales. In the URANS_SSTNL model, the eddy viscosity is attenuated due to the introduction of a nonlinear function of the shear strain rate. The DDES_NL model is switched to the LES mode for the solution in the separation region, thus capturing a richer large-scale turbulent structure. The LES method captures richer turbulent scale information due to the second-order accuracy of the convective term in the center-difference format.

The URANS_SST model cannot simulate the unsteady turbulent flow well, the URANS_SSTNL model can improve the accuracy of the URANS model to some extent, but the accuracy still needs to be improved, while the DDES_NL model shows obvious advantages in the simulation of both scale effects and unsteady flow characteristics.

3.2 Rotational channel

Turbulence in rotating reference systems is of great significance in a range of industrial, geophysical and astrophysical applications. A considerable amount of work has been done to research the influence of system rotation on turbulence. So, the rotational channel flow has also been calculated to further verify the effectiveness of the DDES_NL model as depicted in Fig. 8. The size of the computational domain is $\pi\delta \times 2\delta \times 2\pi\delta$ in the streamwise (x axis), wall-normal (y axis), and spanwise (z axis) directions, respectively, with the $120 \times 120 \times 60$ grid nodes (Zhang *et al.* 2021). The Reynolds number ($\mathrm{Re}_m = 2U_m\delta/\upsilon$, where U_m denoting the friction velocity, δ denoting the channel half-width, and υ denoting the kinematic viscosity) is 5.6×10^3 .The boundary conditions are displayed in Table 3.

The DDES_NL, URANS_SST, URANS_SSTNL models are used to simulate the rotating channel flow. Velocity distribution with different rotation numbers ($Ro = 2|\Omega|\delta/U_m$, 0.15, 0.2, 0.5) is
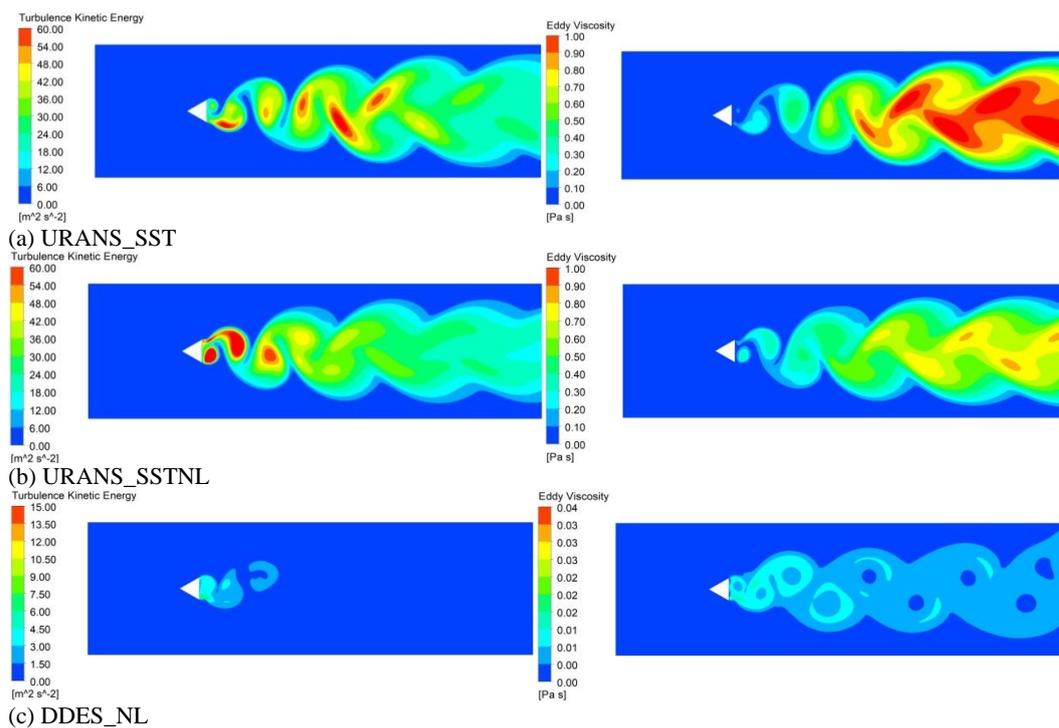

(a) URANS_SST

(b) URANS_SSTNL

(c) DDES_NL

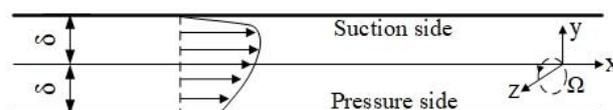**Fig. 7. Eddy viscosity and the turbulence kinetic energy.**

Fig. 8. Sketch of the geometry and mean flow of the channel with spanwise rotation.

Table 3. Boundary conditions for the computational domain.

Boundary	Type	Velocity components	Pressure
Top and bottom	No-slip	$u_i = 0$	$\partial p / \partial n = 0$
Front and back	Symmetry	$\partial u_x / \partial n = \partial u_z / \partial n = 0, u_y = 0$	$\partial p / \partial n = 0$
Inlet and outlet	Periodic	$u_i(x=0,y,z,t) = u_i(x=L_x,y,z,t),$ $\partial u_i / \partial x(x=0,y,z,t) = \partial u_i / \partial x(x=L_x,y,z,t)$	$p(x=0,y,z,t) = p(x=L_x,y,z,t),$ $\partial p / \partial x(x=0,y,z,t) = \partial p / \partial x(x=L_x,y,z,t)$

(a) Ro = 0.15

(b) Ro = 0.2

(c) Ro = 0.5
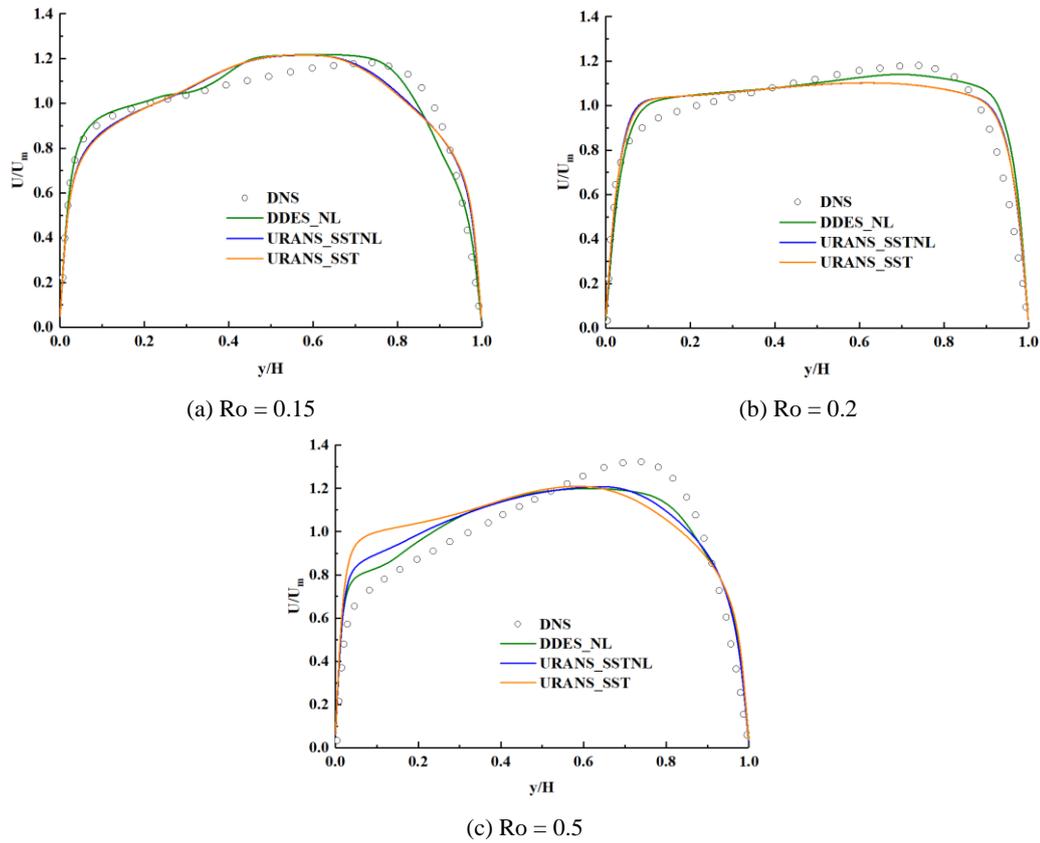
Fig. 9. Velocity distribution.

shown in Fig. 9. It can be seen directly from Fig. 9 that there is a zone near the pressure side where the average velocity has a slope approximately twice the rotation rate of the system. Compared with the direct numerical simulation (DNS) results (Durbin 1991; Zhang *et al.* 2021), the difference between the DDES_NL model and the direct numerical simulation results was found to be small. The important finding is that the URANS method cannot capture the flow characteristics of asymmetric velocity distribution due to rotation in the channel, however, both DDES_NL models can capture such asymmetric flow characteristics.

3.3 Centrifugal pump

Centrifugal pump is a piece of rotating machinery and widely used in many fields, its internal flow not only has typical turbulent characteristics, due to the rotation of the system and the bending of the vanes,

but also has the feature of multi-wall shear rotation of turbulence, so many research scholars have conducted a lot of research on centrifugal pumps. Wang (2019) applied the Curvature-Rotation modified quadratic mean-DES(CRQM-DES) model to the centrifugal pump model and the comparison results show that the simulation is efficient and reliable. Zhang (2019) analyzed the unsteady flow structure of a centrifugal pump and its evolution based on the DDES model, it is clear that the DDES model could precisely capture the flow structure of the model pump. Zhu (2018) adopted the DDES model to investigate the internal pressure pulsation characteristics of the centrifugal pump, the structure, and the evolution of the unsteady vortex in the flow channel. Han (2002) studied the three-dimensional simulation performed for the gas-liquid two-phase turbulent flow in a centrifugal pump with a radial diffuser using the DDES model and mixture

multiphase flow model. Collectively, these studies outline a critical role in verifying the feasibility of applying the DDES model to the centrifugal pump. The internal unsteady flow of centrifugal pumps in this paper has been simulated, 3D structure geometric parameters is shown in Table 4.

Table 4. Some parameters of the centrifugal pump.

Parameters	Value
Flow rate Q_0	100 m^3 /h
Pump head H	32 m
Rotating speed n	1470 r/min
Specific speed n_s	66.7
Blade number Z	7
Inlet diameter of the impeller D_1	94 mm
Outlet diameter of the impeller D_2	314 mm
Volute inlet diameter D_3	324 mm
Volute outlet diameter D_4	125 mm
Blade outlet width b_2	18 mm
Wrap angle ϕ	166.2°
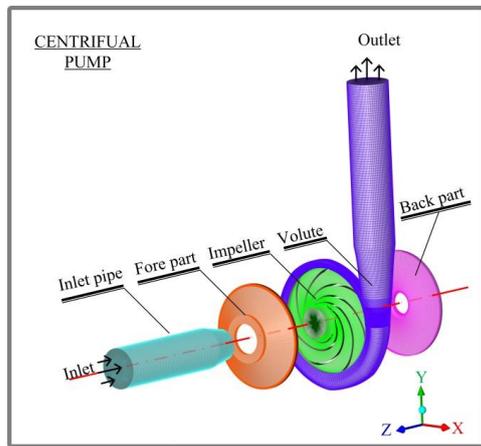
Fig. 10. Computational domain.

Since the advantage of hexahedral meshing is in terms of boundary layer orthogonal, body-fit geometry and numerical dissipation, topology and hexahedral mesh was generated using ANSYS ICEM 15.0 software for the inlet pipe, fore part,

impeller, volute, and impeller back part in the computational domain, respectively, as shown in Fig. 10. Table 5 presents mesh independence analysis. The independence validation has been performed on the five groups of grids. The relative changes in the head were less than 0.5% as the number of grids increased. The total number of grids was eventually determined to be 5 million (Grid 4).

The computational fluid dynamics (CFD) software ANSYS CFX 15 was used to numerically simulate the internal flow of a centrifugal pump under operating conditions ($0.2Q_0$, $0.4Q_0$, $0.6Q_0$, $0.8Q_0$, $1.0Q_0$, and $1.2Q_0$). The Frozen Rotor method is used in the numerical calculation of the steady-state problem to deal with the connection between the dynamic and static part of the regional intersection, and the Transient Rotor Stator method is used in the transient calculation to deal with the dynamic and static intersection. For the specific numerical calculations, the SST model is first used for the steady-state solution, and then the results are used as the initial field for the transient solution. The boundary conditions imposed by the numerical calculation are a given velocity at the inlet, a given pressure at the outlet, and no-slip on the wall. The root means square convergence residual value is set to $1e^{-5}$ and the time step is 0.000113s, which means that the impeller rotates 1 degree in each time step. The total computation time was set at 10 rotation cycles.

Table 6 shows the head at the rated operating condition. The head values estimated by the two models have some differences and are in good agreement with the experimental results. To validate the calculated results, Fig. 11 shows a comparison of the numerical and experimental data. The numerically calculated head and efficiency are by the experimental data over the whole operating range (Zhang *et al.* 2021), which has been done at the experimental base of the 704th Research Institute of China Shipbuilding Industry Corporation and can reflect the hydraulic performance of the centrifugal pump. Therefore, the use of the DDES_NL method to predict the hydraulic performance of the centrifugal pump is feasible.

Table 5. Mesh independence analysis (Unit: million).

	Volute	Inlet pipe	Fore part	Back part	Impeller	Total grid	Head(m)
Grid 1	1.318784	0.704000	0.330880	0.121600	0.410928	2.886192	29.7376
Grid 2	1.318784	0.704000	0.330880	0.121600	1.317078	3.792342	30.6825
Grid 3	1.318784	0.704000	0.397760	0.121600	2.351104	4.893248	31.2543
Grid 4	1.318784	0.704000	0.397760	0.254800	2.351104	5.026448	32.2928
Grid 5	1.318784	0.704000	0.397760	0.254800	3.417792	6.093136	32.1406

Table 6. Comparison of Head prediction.

Numerical Model	DDES_NL	URANS_SST	Experiment(Zhang *et al.* 2021)
Pump Head (m)	32.0669	32.2028	29.9
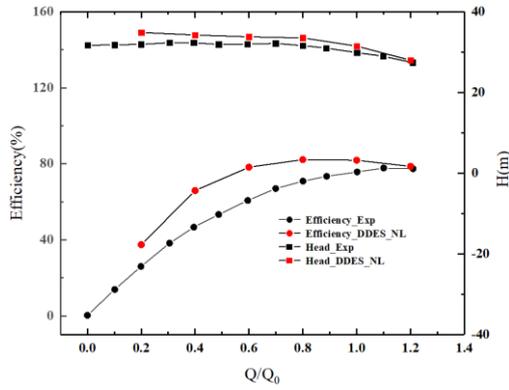
Fig. 11. Head and efficiency curves of the model pump.

The Q criterion rendered by the pressure is utilized to show the three-dimensional characteristics of the vorticity inside the impeller and the volute. As depicted in Fig. 12(a), there is a low-pressure zone in the impeller inlet, and the pressure distribution in each impeller channel is not symmetrical because of the complex flow pattern in the impeller, for example, flow separation. It is indicated that in comparison with the URANS_SST model, the DDES_NL model can capture more abundant flow structures in both the impeller and the volute. This is as a consequence of the URANS_SST model being accurate in solving macro flow, but it cannot accurately capture the small-scale vortex structure existing in the flow field. The velocity distribution in the central section of the two transient methods is
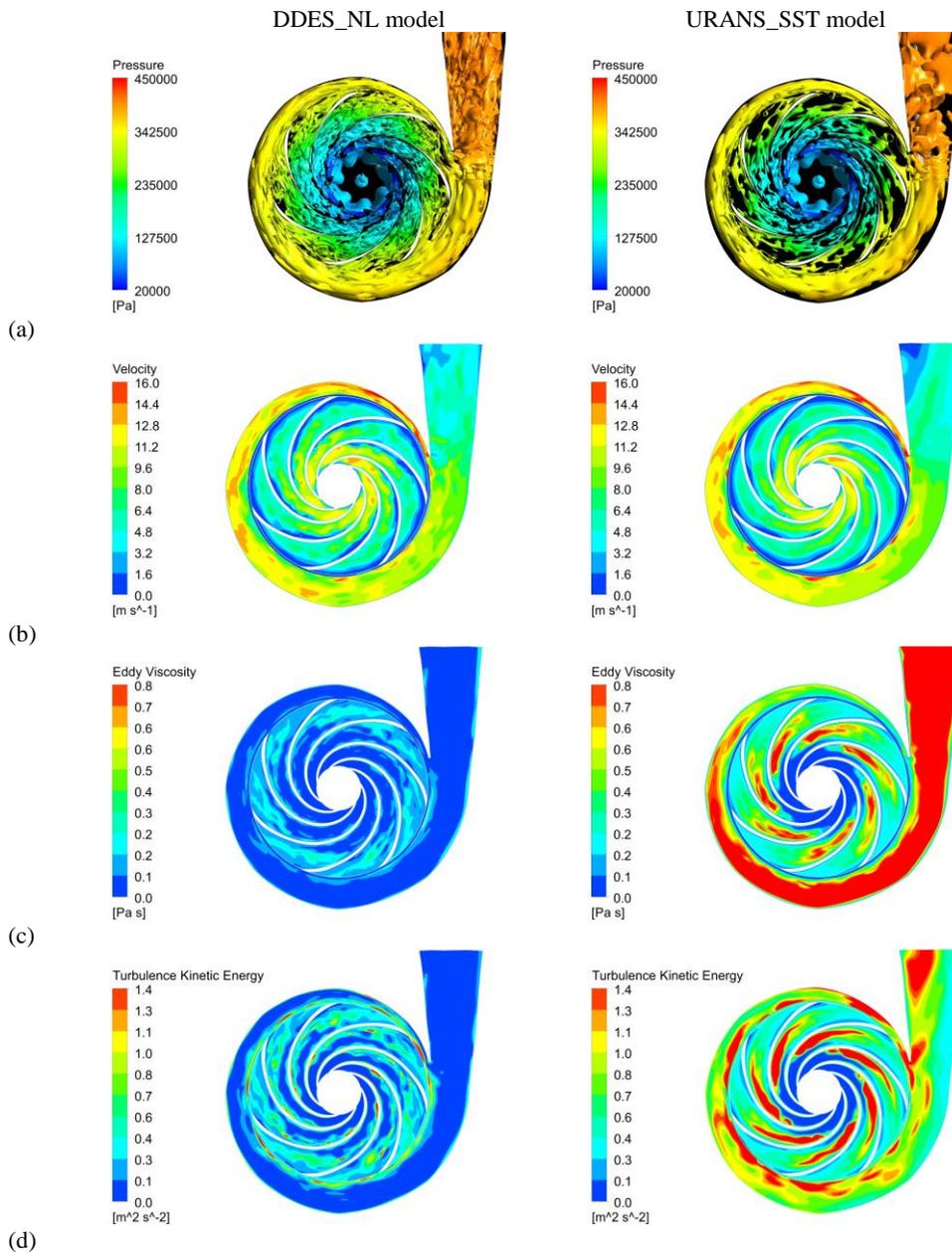
Fig. 12. Distribution contour of turbulent vortex structure, velocity, eddy viscosity and turbulence kinetic energy at $1.0Q_0$.

shown in Fig. 12 (b). The velocity field distribution shows that the velocity field distribution simulated by the two methods is close, but the DDES_NL model can capture the transient flow characteristics of the impeller separation region, while the URANS_SST model the transient velocity field simulated by the model tends to steady-state. The eddy viscosity distribution in the central section of the two transient models is provided in Fig. 12(c). It can be seen that the vortex viscosity coefficient in the DDES_NL model is far less than the URANS_SST model, more turbulent pulsation components are solved directly by momentum equation, so the energy it can capture more abundant turbulence structure scale information. However, in the URANS_SST model, the overall turbulent vorticity is viscous much turbulent small-scale information prematurely attenuates, so only a few regions can be captured free vortex structure. This conclusion corresponds well with Fig. 12(a). The turbulence kinetic energy distribution in the central section of the two transient models in Fig. 12(d). We can observe that in the central region of the impeller channel, the turbulence kinetic energy value is much smaller than that at the trailing edge and in the volute region. At the blade suction side, a relatively high turbulence kinetic energy region is formed. As the wake flow sweeps the volute tongue, the turbulent characteristic would be enhanced as denoted by the high turbulence kinetic energy value. Nevertheless, we also can be seen that the turbulence kinetic energy in the DDES_NL model is much smaller than in the URANS_SST model, which means that the dissipation of fluid energy in the DDES_NL model calculation result is much smaller than the URANS_SST.

Therefore, by comparing the hydraulic performance of the centrifugal pump with the numerical calculation results, it is found that the DDES_NL model can not only obtain the statistical characteristics of centrifugal pumps better, but also capture the internal flow features of centrifugal pumps.

4. CONCLUSION

In this study, a new turbulent model based on Delayed Detached Eddy Simulation with a non-linear eddy viscosity model was developed to predict the complex turbulent flow. Test cases show that the nonlinear turbulence model can extremely improve the simulation accuracy of large separate flows. Calculations for flows around triangular cylinders with unsteady features show that the non-linear eddy viscosity model can improve prediction accuracy to some extent, increase three-dimensional effects and unsteady features. Numerical simulations of a centrifugal pump with a complex structure were performed, and the results showed that the more abundant flow structures inside the centrifugal pump could be better captured. This study shows that the DDES_NL model performs better in simulating the flow field and capturing the non-steady turbulent structure, and can capture the large-scale turbulent structure and the non-steady

flow within an affordable cost, which is an effective method to improve the simulation accuracy.

REFERENCES

Champagne, F., Harris, V. and S. Corrsin (1970). "Experiments on nearly homogeneous turbulent shear flow," *Journal of Fluid Mechanics* 41(1), 81-139.

Chauvet, N., S. Deck and L. Jacquin (2007). Zonal Detached Eddy Simulation of a Controlled Propulsive Jet. *AIAA Journal* 45, 2458-2473.

Du, R., C. Yan, Z. Han, X. Xiang and Qu F. (2017). Performance analysis of DDES delay function in supersonic bottom flow. *Journal of Beijing University of Aeronautics and Astronautics* 43 (08), 1585-1593.

Durbin, P. A. (1991). Near-wall turbulence closure modeling without damping functions, *Theoretical and Computational Fluid Dynamics* 3(1), 1-13.

Froehlich, J. and D. V. Terzi, (2008). Hybrid LES/RANS methods for the simulation of turbulent flows. *Progress in Aerospace Sciences* 44(5), 349-377.

Fu, S., Z. Xiao, H. Chen and J. Huang (2007). Simulation of wing-body junction flows with hybrid RANS/LES methods. *International Journal of Heat and Fluid Flow* 28 (6), 1379-1390.

Han, W., J. Kang, J. Wang, W. Song, C. Chao and F. Wang (2018). The effects of gas fraction on internal flow of centrifugal pump with the vane diffuser. *Journal of Xihua University* (Natural Science Edition) 37(6), 48-53.

Htun, M. (2004). *A study in flow past triangular cylinders with different apex angles*. Doctoral Thesis, National University of Singapore, Singapore.

Hu, J., X. Ning, W. Zhao, F. Li, J. Ma, W. Zhang, S. Sun, M. Zou and C. Lin (2021). Numerical simulation of the cavitating noise of contra-rotating propellers based on detached eddy simulation and the Ffowcs Williams–Hawkings acoustics equation. *Physics of Fluids* 33, 115117.

Hu, O., N. Zhao and W. Shen (2017). Application of SST-DDES model to large separation flow problems. *Journal of Nanjing University of Aeronautics and Astronautics* 49(02), 206-211.

Lee, M. J., Kim, J. and Moin, P. (1990). Structure of turbulence at high shear rate, *Journal of Fluid Mechanics* 216,561-583.

Li, F., C. He, P. Wang and Y. Liu (2021). Unsteady analysis of turbulent flow and heat transfer behind a wall-proximity square rib using dynamic delayed detached-eddy simulation. *Physics of Fluids* 33, 055104.

Lin, D., X. Su and X. Yuan (2016). DDES simulation of high-pressure turbine guide vane. *Journal of Engineering Thermophysics* 37(10), 2085-2088.

Liu, R., A. Hou, S. Shan and F. Ni (2017). Numerical study of non-constant flow of leaf grid separated vortex based on DDES method. *Propulsion Technology* 38(1), 17-26.

Liu, Y. and M. Tong (2015). Aerodynamic noise simulation analysis of cavity with/without hatch based on DDES. *Aviation Computing Technology* 45(03), 30-34.

Ma, Z., S. Huang and D. Zhu (2009). Study on applicability of turbulenc model in ship computational fluid dynamics. *Chinese Journal of Hydrodynamics* 24(2), 207-216.

Menter, F, R. and Y. Egorov (2010). The scale-adaptive simulation method for unsteady turbulent flow predictions. Part 1: Theory and model description. *Flow Turbulence and Combustion* 85(1), 113-138.

Menter, F. and M. Kuntz (2003). A Zonal SST-DES Formulation. *In: DES-WORKSHOP, St. Petersburg Technical University*.

Rogers, M. M. and P. Moin (1987). The structure of the vorticity field in homogeneous turbulent flows, *Journal of Fluid Mechanics* 176, 33-66.

Shi, Y. and W. Kollmann (2021). Improved Delayed Detached Eddy Simulation of a Porous Wavy Trailing Edge. *Physics of Fluids* 33(5), 055128.

Sjunnesson, A., R. Henriksson and C. Lofstrom, (1992): CARS measurements and visualization of reacting flows in bluff body stabilized flame. *AIAA Paper*. 92-3650.

Spalart, P. R. (2009). Detached-eddy simulation. *Annual Review of Fluid Mechanics* 41,181-202.

Spalart, P. R., S. Deck, M. L. Shur, K. D. Squires, M. Kh. Strelets and A. Travin (2006). A New Version of Detached-eddy Simulation, Resistant to Ambiguous Grid Densities. *Theoretical and Computational Fluid Dynamics* 20(3), 181-195.

Spalart, P. R., W. H. Jou and M. Strelets (1997). Comments on the feasibility of LES for wings and on a hybrid RANS/LES approach//*Proceedings of 1st AFOSR International Conference on DNS/LES,Advances in DNS /LES. Columbus: Greyden Press* 137-147.

Strelets, M. (2001). Detached eddy simulation of massively separated flows// *Aiaa Fluid Dynamics Conference & Exhibit,* 1-18.

Tavoularis, S. and S. Corrsin (1981). Experiments in nearly homogenous turbulent shear flow with a uniform mean temperature gradient. Part 1, *Journal of Fluid Mechanics* 104,311-347.

Trapier, S., S. Deck and P. Duveau (2008). Delayed Detached-Eddy Simulation and Analysis of Supersonic Inlet Buzz. *AIAA Journal,* 46(1), 118-131.

Travin, A., Shur, M., Strelets, M. and P. Spalart (2000). Detached-Eddy Simulations Past a Circular Cylinder. *Flow Turbulence and Combustion* 63, 293-313.

Tucker, P. G. (2011a). Computation of unsteady turbomachinery flows: Part 1–Progress and challenges. *Progress in Aerospace Sciences* 47(7), 522-545.

Tucker, P. G. (2011b). Computation of unsteady turbomachinery flows: Part 2–LES and hybrids. *Progress in Aerospace Sciences* 47(7), 546-569.

Vengadesan, S. and P. Nithiarasu (2007). Hybrid LES-review and assessment. *Sadhana,* 32(5), 501-511.

Wang, Y. (2019). *Improvement and Application of RANS/LES Turbulence Model Based on Turbulent Flow Field with Curvature and Rotation Effect*. Jiangsu University, Zhenjiang, China.

Wei, Q. (2017), *Study on the characteristics and impact mechanism of pressure fluctuation in a centrifugal pump with gap drainage blades* Doctoral Thesis, Shanghai University, Shanghai, China.

Wei, Q., H. Chen and Z. Ma (2015). Numerical Simulation of Flow around Airfoil with Non-Linear RANS Model, Proc. ASME/JSME/KSME 2015 Joint Fluids Engineering Conference, *American Society of Mechanical Engineers* V01AT02A014-V001AT002A014.

Wei, Q., H. Chen and Z. Ma (2016). An hybrid RANS/LES model for simulation of complex turbulent flow, *Journal of Hydrodynamics* 28(5), 811-820.

Yin, Z. and K. R. Reddy and P. A. Durbin (2015). On the dynamic computation of the model constant in delayed detached eddy simulation. *Physics of Fluids* 27(2), 025105.

Zhang, H., J. Yang, L. Xiao and H. Lu (2015). Large-eddy simulation of flow past both finite and infinite circular cylinders at Re = 3900. *Journal of Hydrodynamics* 27(2), 195-203.

Zhang, J., Y. Ai, D, Huang and J. Liu (2016). Numerical simulation study of interference in a triangular wing large-angle wind tunnel test stand. *Journal of Aeronautics* 37(08), 2481-2489.

Zhang, K., Y. Jin, X. Han and X. He (2022). Very-

Large-Eddy Simulation of Nonreactive Turbulent Flow for Annular Trapped Vortex Combustor. *Journal of Applied Fluid Mechanics* 15(2), 523-535.

Zhang, N., X. Liu, B. Gao and B. Xia (2019). DDES analysis of the unsteady wake flow and its evolution of a centrifugal pump. *Renewable Energy* 141, 570-582.

Zhang, Z., H. Chen, Z. Ma, J. He and C. Liu (2019a). Research on Improving the Dynamic Performance of Centrifugal Pumps with Twisted Gap Drainage Blades. *Journal of Fluids Engineering* 141(9), 1-15.

Zhang, Z., H. Chen, Z. Ma, Q. Wei, J. He, H. Liu and C. Liu (2019b). Application of the hybrid RANS/LES method on the hydraulic dynamic performance of centrifugal pumps. *Journal of Hydrodynamics* 31(3), 637-640.

Zhang, W., Y. Yu and H. Chen (2010). The turbulence simulation of off-design condition in centrifugal impellers. *Journal of Drainage and Irrigati Machinery Engineering* 28(1), 38-42.

Zhang, Z., H. Chen, J. Yin, Z. Ma, Q. Gu, J. Lu and H. Liu (2021). Unsteady flow characteristics in centrifugal pump based on proper orthogonal decomposition method. *Physics of Fluids* 33(7), 075122.

Zhu, B. (2014). *Research on the mechanism of performance improving in low specific speed centrifugal pump with gap drainage blades*. Doctoral Thesis, Shanghai University, Shanghai, China.

Zhu, B., H. Chen and Q. Wei (2014). Numerical and experimental investigation of cavitating characteristics in centrifugal pump with gap impeller. *International Journal of Turbo and Jet-Engines* 31(1), 1-10.

Zhu, Y. (2018). *Study on unsteady vortex characteristics of centrifugal pump based on DDES model*. Lanzhou University of Technology, Lanzhou, China.